Available online at www.sciencedirect.com
SCIENCE DIRECT®
International Journal of Heat and Mass Transfer 47 (2004) 5139–5148
International Journal of HEAT and MASS TRANSFER
www.elsevier.com/locate/ijhmt

Prediction of the entrainment of ambient air into a turbulent argon plasma jet using a turbulence-enhanced combined-diffusion-coefficient method

Kai Cheng, Xi Chen *

Department of Engineering Mechanics, Tsinghua University, Beijing 100084, PR China

Received 2 January 2004; received in revised form 11 May 2004
Available online 21 August 2004

Abstract

The entrainment of the ambient air into a turbulent argon plasma jet is studied numerically using a turbulence-enhanced combined-diffusion-coefficient method. Namely, the Navier–Stokes equations and two-equation turbulence model coupled with the turbulence-enhanced combined-diffusion-coefficient approach are employed to predict the turbulent plasma jet characteristics including the evolution of air mole fraction along the plasma jet in air surroundings. Although complicated gas species always exist in the plasma jet due to rather high gas temperatures being involved, it is shown that the entrainment of ambient air into the turbulent argon plasma jet can still be treated simply by the combined turbulent and molecular diffusion between only two different gases (argon and air). Good agreement between the predicted results with corresponding experimental data reported by Fincke et al. [Int. J. Heat Mass Transfer 46 (22) (2003) 4201] demonstrates the applicability of the present modeling approach.
© 2004 Elsevier Ltd. All rights reserved.

Keywords: Thermal plasma; Turbulent argon jet; Air entrainment; Turbulence-enhanced combined-diffusion-coefficient method

1. Introduction

Thermal plasmas have been widely employed as the high temperature energy sources in many applications, such as the plasma spraying, thermal plasma chemical vapor deposition, thermal plasma synthesis, thermal plasma waste destruction, cladding or remelting of materials surface, etc. [1,2]. In most of the practical applications, the high-temperature partially-ionized gas generated in a plasma torch is ejected from the torch in the form of a plasma jet. Numerous studies have been conducted in the past decades concerning the plasma jet characteristics, but most of them are concerned with turbulent plasma jets, cf. Refs. [2–9] and the references cited therein.

Long laminar plasma jets have been successfully generated in recent years by use of elaborately designed plasma torches [10–12]. It has been shown that in comparison with the turbulent plasma jets, the entrainment of ambient air into the laminar plasma jet is appreciably weakened, resulting in much longer high-temperature region length and appreciably smaller axial gradients of plasma temperature and velocity within the jet.

* Corresponding author. Tel.: +86 10 62772924/62773781; fax: +86 10 62781824.
E-mail address: cx-dem@mail.tsinghua.edu.cn (X. Chen).

0017-9310/$ - see front matter © 2004 Elsevier Ltd. All rights reserved.
doi:10.1016/j.ijheatmasstransfer.2004.06.028

Nomenclature

C_1, C_2, C_μ	turbulence model constants
c_p	specific heat at constant pressure ($J\,kg^{-1}\,K^{-1}$)
$\overline{D}^x_{AB}$	combined ordinary diffusion coefficient ($m^2\,s^{-1}$)
$\overline{D}^T_{AB}$	combined thermal diffusion coefficient ($kg\,m^{-1}\,s^{-1}$)
f	mass fraction
h	specific enthalpy ($J\,kg^{-1}$)
J	diffusion mass flux vector ($kg\,m^{-2}\,s^{-1}$)
K	turbulent kinetic energy ($m^2\,s^{-2}$)
m	particle mass (kg)
$\bar{m}$	average mass of all the heavy particles (excluding electrons) (kg)
$\overline{M}$	average mass of all the gas particles (including electrons) (kg)
n	gas particle number density (m^{-3})
p	pressure (Pa)
Pr	turbulent Prandtl number
R_{in}	plasma jet inlet (or torch exit) radius (m)
r	radial coordinate (m)
S_f	source term in species diffusion equation ($kg\,m^{-3}\,s^{-1}$)
Sc	turbulent Schmidt number
T	temperature (K)
T_0	maximum temperature at jet inlet (K)
U_0	maximum axial velocity at jet inlet ($m\,s^{-1}$)
U_r	radiation power loss per unit volume of plasma ($W\,m^{-3}$)
u	axial velocity component ($m\,s^{-1}$)
v	radial velocity component ($m\,s^{-1}$)
X	mole fraction
x	axial coordinate (m)

Greek symbols

$\delta_{0.1}$	jet width (m)
Γ_f	transport coefficient for molecular diffusion ($kg\,m^{-1}\,s^{-1}$)
ε	turbulence dissipation rate ($m^2\,s^{-3}$)
μ	viscosity (Pa s)
ρ	mass density ($kg\,m^{-3}$)
ϕ	dependent variable

Subscripts

0	centerline
A	gas A (argon)
B	gas B (air)
f	about mass fraction
h	about enthalpy
in	torch nozzle inner wall; jet inlet
K	about turbulent kinetic energy
out	torch nozzle outer wall
r	radial direction
x	axial direction
ε	about turbulence dissipation rate

Appreciable decrease in ambient air entrainment represents a marked merit of the long laminar plasma jet, since the existence of air species in plasma jets would cause the undesired oxidation of metallic particles injected into the plasma jet and of the metallic workpiece exposed to the plasma jet. With the recent development in long laminar plasma jet generation technology [10–12] as the research background, Xu et al. [13] performed a modeling study concerning the characteristics of the long laminar argon plasma jet issuing into ambient air. Especially, they studied numerically the diffusion of the ambient air into the laminar argon plasma jet. The combined-diffusion-coefficient method suggested by Murphy [14,15] was employed in Ref. [13] to study the entrainment of ambient air into the long laminar argon plasma jet. The modeling results showed that although the entrainment of ambient air into the long laminar argon plasma jet was appreciably less than that for the turbulent plasma jet case due to only molecular diffusion mechanism being involved in the laminar jet, considerably large air contents could still exist in the long laminar plasma jet, especially in its downstream region far from the jet inlet. The correctness of predicted results of Ref. [13] concerning the entrainment of ambient air into the plasma jet has not been quantitatively checked due to the lack of corresponding experimental data, although according to Murphy's opinion [15], his combined-diffusion-coefficient method is equivalent to the full multicomponent diffusion treatment for the local chemical equilibrium case and thus it should be able to give good prediction.

With the plasma spraying as the research background, recently Fincke and his collaborators [16] report their experimental results concerning the characteristics of a turbulent argon plasma jet issuing into the ambient air. Enthalpy probe, high-resolution Thomson scattering, laser induced fluorescence, coherent anti-Stokes Raman spectroscopy and other diagnostic tools were used in their measurements to determine the velocity, temperature and species concentration distributions in the plasma jet. At the same time, they also performed a modeling study on the jet characteristics [17] using

the computer program LAVA developed in their group. In their modeling work, turbulence had been treated using the ordinary K–ε two-equation turbulence model. Neutrals, ions and electrons were considered as separate components of the mixture, and they used general kinetic and equilibrium chemistry algorithms to compute ionization, dissociation, recombination and other chemical reactions for the species diffusion study. The modeling results concerning the entrained air contents (%) were compared with their own experimental data. It was found that when the turbulence parameters at the jet inlet were appropriately calculated, good agreement could be achieved between their predicted results and corresponding experimental data [17].

The characteristics of the same turbulent argon plasma jet as studied in [16,17] are re-examined in this paper using a modeling approach somewhat different from that employed by the authors of Ref. [17]. Similarly to the combined-diffusion-coefficient method previously used to treat the species diffusion in laminar plasma flows [13–15], the turbulence-enhanced combined-diffusion-coefficient method is used in the present study to predict the entrainment of ambient air into the argon plasma jet. This approach is much simpler than that used in [17], since only the treatment of the diffusion between two different gases is required. The predicted results using the new approach will also be compared with the experimental data of Fincke et al. [16] to check the applicability of the proposed modeling approach, especially to check the applicability of the combined-diffusion-coefficient method [13–15] to some extent.

2. Modeling approach

Plasma flow and heat/mass transfer in the turbulent plasma jet are always coupled with each other. Hence, the study of the entrainment of the ambient air into the turbulent argon plasma jet must be treated as a part of the study concerning the turbulent plasma jet characteristics.

2.1. Basic assumptions

Basic assumptions employed in the present study include:

(1) The plasma jet flow is axi-symmetrical and steady in a time-averaged sense;
(2) The plasma is in the local thermodynamic equilibrium (LTE) and local chemical equilibrium (LCE) state, and thus all the gas properties are temperature- and composition-dependent;
(3) The plasma is optically thin to radiation;
(4) The swirling velocity components in the plasma jet can be neglected;
(5) The K–ε two-equation turbulence model can be employed to study the turbulence;
(6) All the current-related terms in momentum and energy equations, including the Lorentz force, Joule heating rate and electron enthalpy transport terms, can be ignored for the whole plasma jet region.

Except for Assumption (2), all the other assumptions listed above are the same as those used or actually used by [17]. It is expected that Assumption (2) is also a good approximation for the plasma jet due to rather high gas temperatures being involved.

2.2. Governing equations

Based on the foregoing assumptions, the governing equations can be written in a cylindrical coordinate $(x-r)$ system as follows [13,18].

Continuity equation

$$\frac{\partial}{\partial x}(\rho u)+\frac{1}{r}\frac{\partial}{\partial r}(r\rho v)=0 \tag{1}$$

Axial (x-) momentum conservation equation

$$\begin{aligned}&\frac{\partial(\rho uu)}{\partial x}+\frac{1}{r}\frac{\partial(r\rho uv)}{\partial r}\\&\quad=-\frac{\partial p}{\partial x}+2\frac{\partial}{\partial x}\left[(\mu+\mu_{\mathrm{T}})\frac{\partial u}{\partial x}\right]\\&\qquad+\frac{1}{r}\frac{\partial}{\partial r}\left[r(\mu+\mu_{\mathrm{T}})\left(\frac{\partial u}{\partial r}+\frac{\partial v}{\partial x}\right)\right]\end{aligned} \tag{2}$$

Radial (r-) momentum conservation equation

$$\begin{aligned}&\frac{\partial(\rho uv)}{\partial x}+\frac{1}{r}\frac{\partial(r\rho vv)}{\partial r}\\&\quad=-\frac{\partial p}{\partial r}+\frac{2}{r}\frac{\partial}{\partial r}\left[r(\mu+\mu_{\mathrm{T}})\frac{\partial v}{\partial r}\right]\\&\qquad+\frac{\partial}{\partial x}\left[(\mu+\mu_{\mathrm{T}})\left(\frac{\partial v}{\partial x}+\frac{\partial u}{\partial r}\right)\right]-2(\mu+\mu_{\mathrm{T}})\frac{v}{r^2}\end{aligned} \tag{3}$$

Energy conservation equation

$$\begin{aligned}&\frac{\partial(\rho uh)}{\partial x}+\frac{1}{r}\frac{\partial(r\rho vh)}{\partial r}\\&\quad=\frac{\partial}{\partial x}\left[\left(\frac{k}{c_{\mathrm{p}}}+\frac{\mu_{\mathrm{T}}}{\mathrm{Pr}_{\mathrm{h}}}\right)\frac{\partial h}{\partial x}\right]+\frac{1}{r}\frac{\partial}{\partial r}\left[r\left(\frac{k}{c_{\mathrm{p}}}+\frac{\mu_{\mathrm{T}}}{\mathrm{Pr}_{\mathrm{h}}}\right)\frac{\partial h}{\partial r}\right]\\&\qquad-U_{\mathrm{r}}-\frac{\partial}{\partial x}[(h_{\mathrm{A}}-h_{\mathrm{B}})J_x]-\frac{1}{r}\frac{\partial}{\partial r}[r(h_{\mathrm{A}}-h_{\mathrm{B}})J_{\mathrm{r}}]\\&\qquad-\frac{\partial}{\partial x}\left[\frac{k}{c_{\mathrm{p}}}(h_{\mathrm{A}}-h_{\mathrm{B}})\frac{\partial f_{\mathrm{A}}}{\partial x}\right]-\frac{1}{r}\frac{\partial}{\partial r}\left[r\frac{k}{c_{\mathrm{p}}}(h_{\mathrm{A}}-h_{\mathrm{B}})\frac{\partial f_{\mathrm{A}}}{\partial r}\right]\end{aligned} \tag{4}$$

Species conservation equation

$$\begin{aligned}&\frac{\partial(\rho uf_{\mathrm{A}})}{\partial x}+\frac{1}{r}\frac{\partial(r\rho vf_{\mathrm{A}})}{\partial r}\\&\quad=\frac{\partial}{\partial x}\left[\left(\frac{\mu_{\mathrm{T}}}{Sc_{\mathrm{f}}}+\Gamma_{\mathrm{f}}\right)\frac{\partial f_{\mathrm{A}}}{\partial x}\right]+\frac{1}{r}\frac{\partial}{\partial r}\left[r\left(\frac{\mu_{\mathrm{T}}}{Sc_{\mathrm{f}}}+\Gamma_{\mathrm{f}}\right)\frac{\partial f_{\mathrm{A}}}{\partial r}\right]+S_{\mathrm{f}}\end{aligned} \tag{5}$$

Turbulent kinetic energy equation

$$\frac{\partial(\rho u K)}{\partial x}+\frac{1}{r}\frac{\partial(rv\rho K)}{\partial r} = \frac{\partial}{\partial x}\left[\left(\mu+\frac{\mu_{\mathrm{T}}}{\mathrm{Pr}_K}\right)\frac{\partial K}{\partial x}\right]+\frac{1}{r}\frac{\partial}{\partial r}\left[r\left(\mu+\frac{\mu_{\mathrm{T}}}{\mathrm{Pr}_K}\right)\frac{\partial K}{\partial r}\right]+G-\rho\varepsilon \tag{6}$$

Turbulence dissipation rate equation

$$\frac{\partial(\rho u\varepsilon)}{\partial x}+\frac{1}{r}\frac{\partial(rv\rho\varepsilon)}{\partial r} = \frac{\partial}{\partial x}\left[\left(\mu+\frac{\mu_{\mathrm{T}}}{\mathrm{Pr}_\varepsilon}\right)\frac{\partial\varepsilon}{\partial x}\right]+\frac{1}{r}\frac{\partial}{\partial r}\left[r\left(\mu+\frac{\mu_{\mathrm{T}}}{\mathrm{Pr}_\varepsilon}\right)\frac{\partial\varepsilon}{\partial r}\right] +\frac{\varepsilon}{K}(C_1G-C_2\rho\varepsilon) \tag{7}$$

In the foregoing equations, all the physical quantities are their time-averaged values. ρ, μ, k, h and c_{p} are the temperature- and composition-dependent gas density, viscosity, thermal conductivity, specific enthalpy and specific heat at constant pressure; p and f_{A} the gas pressure and the mass fraction of argon in the argon–air mixture; u and v the axial (x-) and radial (r-) components of velocity vector; whereas K and ϵ are the turbulent kinetic energy and its dissipation rate, respectively. μ_{T} is the turbulent viscosity and is calculated by $\mu_{\mathrm{T}}=C_\mu\rho K^2/\varepsilon$, whereas C_μ, C_1, C_2, Pr_{h}, Sc_{f}, Pr_K and Pr_ε are constants in the turbulence model, and in this study they are taken to be their commonly adopted values, i.e. 0.09, 1.44, 1.92, 0.9, 1.0, 1.0 and 1.3, respectively. The turbulence generation term, G, in Eqs. (6) and (7) is

$$G=\mu_{\mathrm{t}}\left[2\left(\frac{\partial v}{\partial r}\right)^2+2\left(\frac{\partial u}{\partial x}\right)^2+2\left(\frac{v}{r}\right)^2+\left(\frac{\partial u}{\partial r}+\frac{\partial v}{\partial x}\right)^2\right] \tag{8}$$

whereas the source term, S_{f}, in the species conservation equations (5) can be written as [13,18]

$$S_{\mathrm{f}}=\frac{\partial}{\partial x}\left(\Gamma_{\mathrm{f}}\frac{f_{\mathrm{A}}}{\overline{M}}\frac{\partial\overline{M}}{\partial x}\right)-\frac{\partial}{\partial x}\left(\Gamma_{\mathrm{f}}\frac{f_{\mathrm{A}}}{\overline{M}_{\mathrm{A}}}\frac{\partial\overline{M}_{\mathrm{A}}}{\partial x}\right) +\frac{1}{r}\frac{\partial}{\partial r}\left(r\Gamma_{\mathrm{f}}\frac{f_{\mathrm{A}}}{\overline{M}}\frac{\partial\overline{M}}{\partial r}\right)-\frac{1}{r}\frac{\partial}{\partial r}\left(r\Gamma_{\mathrm{f}}\frac{f_{\mathrm{A}}}{\overline{M}_{\mathrm{A}}}\frac{\partial\overline{M}_{\mathrm{A}}}{\partial r}\right) +\frac{\partial}{\partial x}\left(\overline{D}^{\mathrm{T}}_{\mathrm{AB}}\frac{\partial\ln T}{\partial x}\right)+\frac{1}{r}\frac{\partial}{\partial r}\left(r\overline{D}^{\mathrm{T}}_{\mathrm{AB}}\frac{\partial\ln T}{\partial r}\right) \tag{9}$$

In energy equation (4), all the terms involving $(h_{\mathrm{A}}-h_{\mathrm{B}})$ are added in order to include the energy transport caused by the species diffusion [13,18]. U_{r} is the temperature- and composition-dependent radiation power per unit volume of the plasma, h_{A} and h_{B} are the specific enthalpies of pure argon and pure air, respectively, whereas J_x and J_{r} are the x- and r- components of the following diffusion mass flux vector of argon species

$$\vec{J}_{\mathrm{A}}=-\left(\frac{\mu_{\mathrm{T}}}{Sc_{\mathrm{f}}}\right)\nabla f_{\mathrm{A}}-(n^2/\rho)\bar{m}_{\mathrm{A}}\bar{m}_{\mathrm{B}}\overline{D}^{x}_{\mathrm{AB}}\nabla X_{\mathrm{A}}-\overline{D}^{\mathrm{T}}_{\mathrm{AB}}\nabla\ln T \tag{10}$$

Here n is the total gas-particle number density. $\bar{m}_{\mathrm{A}}$ and $\bar{m}_{\mathrm{B}}$ are the averaged gas-particle mass for all the *heavy* particles (excluding electrons) coming from argon (i.e. species A) and those coming from air (i.e. species B), X_{A} is the mole fraction of argon in the argon–air mixture, whereas $\overline{D}^{x}_{\mathrm{AB}}$ and $\overline{D}^{\mathrm{T}}_{\mathrm{AB}}$ are the combined ordinary diffusion coefficient associated with the mole-concentration gradient ∇X_{A} and the combined thermal diffusion coefficient associated with the temperature gradient ∇T, respectively [14,15]. The molecular part of the transport coefficient in Eq. (5) is represented by

$$\Gamma_{\mathrm{f}}=\left[\bar{m}_{\mathrm{A}}\bar{m}_{\mathrm{B}}/(\overline{M}\overline{M}_{\mathrm{A}})\right]\rho\overline{D}^{x}_{\mathrm{AB}} \tag{11}$$

in which $\overline{M}$ and $\overline{M}_{\mathrm{A}}$ are the averaged particle mass for all the gas particles (including electrons) in the argon–air mixture and that for those coming from argon, respectively [13–15,18].

Some words should be added here concerning the employment of turbulence-enhanced combined-diffusion-coefficient method embodied in Eq. (5). When the combined-diffusion-coefficient method is used to treat the diffusion in the argon–air mixture when *only* molecular diffusion mechanism is considered (e.g. for the laminar plasma jet case), the following specie conservation equation can be constructed [13,18]

$$\frac{\partial(\rho u f_{\mathrm{A}})}{\partial x}+\frac{1}{r}\frac{\partial(r\rho v f_{\mathrm{A}})}{\partial r}=\frac{\partial}{\partial x}\left(\Gamma_{\mathrm{f}}\frac{\partial f_{\mathrm{A}}}{\partial x}\right)+\frac{1}{r}\frac{\partial}{\partial r}\left(r\Gamma_{\mathrm{f}}\frac{\partial f_{\mathrm{A}}}{\partial r}\right)+S_{\mathrm{f}} \tag{12}$$

in which Γ_{f} and S_{f} are given by Eqs. (11) and (9), respectively. On the other hand, if *only* turbulent diffusion mechanism is considered for the argon–air mixture, the following specie conservation equation can be employed:

$$\frac{\partial(\rho u f_{\mathrm{A}})}{\partial x}+\frac{1}{r}\frac{\partial(r\rho v f_{\mathrm{A}})}{\partial r}=\frac{\partial}{\partial x}\left[\left(\frac{\mu_{\mathrm{T}}}{Sc_{\mathrm{f}}}\right)\frac{\partial f_{\mathrm{A}}}{\partial x}\right]+\frac{1}{r}\frac{\partial}{\partial r}\left[r\left(\frac{\mu_{\mathrm{T}}}{Sc_{\mathrm{f}}}\right)\frac{\partial f_{\mathrm{A}}}{\partial r}\right] \tag{13}$$

The species conservation equation (5) can thus be constructed as the combination of Eqs. (12) and (13) for the present case in which *both* molecular and turbulent diffusion mechanisms are involved. Since both turbulent and molecular diffusion mechanisms are included in Eq. (5) and the molecular diffusion has been treated by use of the combined-diffusion-coefficient method [14,15], this approach to treat the simultaneous turbulent and molecular diffusion can be called the turbulence-enhanced combined-diffusion-coefficient method. It is noted that the effect of temperature gradient on the species diffusion has been included in the present approach. This effect is

not only through the ordinary thermal diffusion (usually small), but more importantly also through the variation of mole fraction X_A or X_B with plasma temperature [14,15].

2.3. Computational domain and boundary conditions

The computational domain for this study is taken to be the region A–B–C–D–E–F–A shown in Fig. 1. The inner radius (R_{in}) of the torch exit or the jet inlet radius (AB in Fig. 1) is 4 mm, whereas the outer radius (R_{out}) of the torch wall (BC) is 35 mm. The axial length AF and the radial width AD of the computational domain are taken to be 100 mm and 40 mm, respectively. 124 (x-direction) × 78 (r-direction) non-uniform grid points are adopted in the computation with finer grid spacing near the jet inlet and the jet axis.

Boundary conditions employed in this study are as follows:

(i) At the jet inlet (or torch exit) AB, the following axial velocity and temperature profiles as used in [17] are adopted:

$$u_{in} = U_0[1-(r/R_{in})^{1.4}],\quad T_{in} = (T_0 - T_w)[1-(r/R_{in})^{2.3}] + T_w \tag{14}$$

in which T_w is the torch inner-wall temperature and T_w = 700 K. In addition, $v = 0$, $f_A = 1.0$,

$$K = 0.00005 \times u_{in}^2 \tag{15}$$

and $\varepsilon = K^{\frac{3}{2}}/L$ are used, where $L = 0.075\delta_{0.1}/C_\mu^{3/4}$, whereas $\delta_{0.1}$ is the jet width defined by the radial distance at which the axial velocity reduces to $u = 0.1U_0$ [17].

(ii) Along the wall surface BC, zero diffusion flux and turbulence-wall-functions are used. The temperatures in radial direction along the wall surface are assumed to satisfy the distribution $T = 700 - 400\frac{\ln(r/R_{in})}{\ln(R_{out}/R_{in})}$ (the temperature at the upper end of the wall is taken to be 300 K) [17].

(iii) Boundary conditions $\partial u/\partial x = 0$, $\partial v/\partial x = 0$, T = 300 K, $f_A = 0$, $K = 0$ and $\varepsilon = 0$ are used at the vertical free boundary CD.

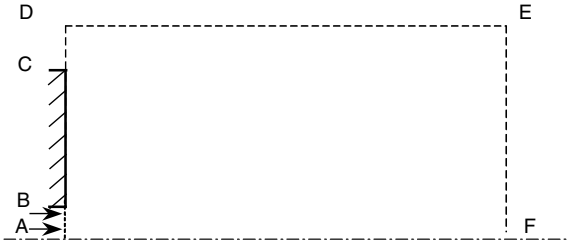

Fig. 1. Computational domain used in this study.

(iv) Boundary conditions $\partial u/\partial r = 0$, $\partial(\rho r v)/\partial r = 0$ T = 300 K, $f_A = 0$, $K = 0$ and $\varepsilon = 0$ are used along the top free boundary DE.

(v) One-way conditions are adopted at the downstream boundary EF, i.e. $\partial\phi/\partial x = 0$ ($\phi = u, v, h, f_A, K, \varepsilon$).

(vi) Along the jet axis AF, axi-symmetrical conditions are employed for the present two-dimensional simulation, i.e. $\partial\phi/\partial r = 0$ ($\phi = u, h, f_A, K, \varepsilon$) and $v = 0$.

In the present modeling, the same jet inlet temperature and axial velocity profiles (14) with T_0 = 12913 K and U_0 = 1092 m/s as used in [17] are employed to facilitate the comparison between the present modeling results with the experimental data presented by Fincke et al. [16]. It is found that when those inlet profiles and the inlet turbulent kinetic energy expression (15) are used, the computed plasma temperature and axial velocity distributions at the cross section 2 mm downstream from the jet inlet agree well with the experimental data presented in [17] for the turbulent argon plasma jet ejected from a Miller SG-100 spray torch into ambient air (torch arc current 900 A, arc voltage 15.4 V, argon flow rate 2.1 STP m^3/h and thermal efficiency of 70%).

3. Results and discussion

In our modeling work, the SIMPLE algorithm [19] has been employed to solve simultaneously the governing equations (1)–(7). After the values of the argon mass fraction f_A in the argon–air mixture have been computed, corresponding argon mole fraction X_A, air mass fraction f_B and air mole fraction X_B can be easily calculated, respectively, from the following relations

$$f_A = m_A X_A/[m_B + (m_A - m_B)X_A] \tag{16}$$

$$f_B = 1 - f_A \tag{17}$$

$$f_B = m_B X_B/[m_A - (m_A - m_B)X_B] \tag{18}$$

On the other hand, although the specific enthalpy has been used as the dependent variable to be solved in the energy equation (4), it can also be easily converted to temperature, since the specific enthalpy is a function of plasma temperature and gas composition for the LTE and LCE case.

Figs. 2–7 present some modeling results concerning the turbulent plasma jet characteristics, including the distributions of the plasma axial velocity, temperature, argon mass fraction, turbulent kinetic energy, turbulence dissipation rate and turbulent/molecular viscosity ratio in the plasma jet.

In comparison with the long laminar argon plasma jet studied in [13], Figs. 2–4 show that the turbulent

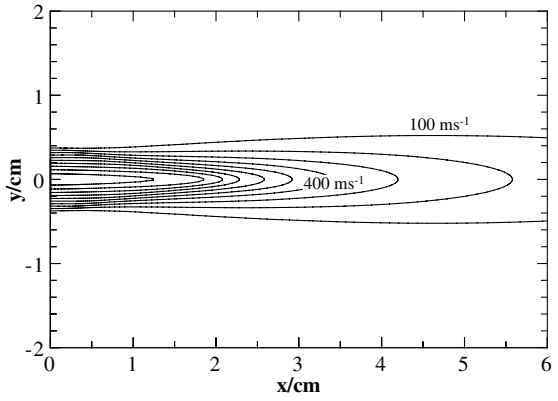

Fig. 2. Computed spatial distribution of the axial velocity contours in the plasma jet (outer line—100 $m\,s^{-1}$, contour interval—100 $m\,s^{-1}$; $y < 0$—lower semi-plane, $y > 0$—upper semi-plane).

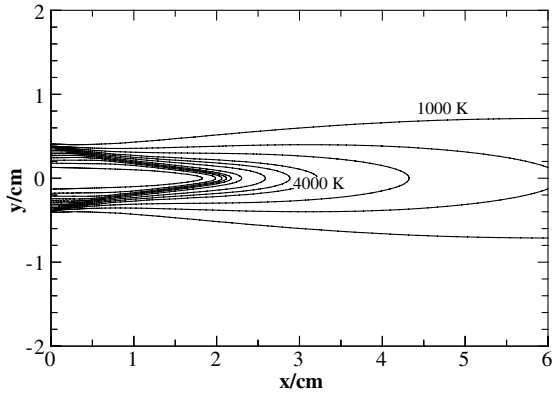

Fig. 3. Computed isotherm distribution in the plasma jet (outer line—1000 K, isotherm interval—1000 K; $y < 0$—lower semi-plane, $y > 0$—upper semi-plane).

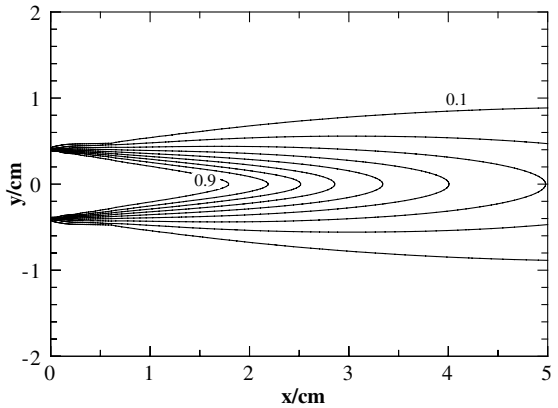

Fig. 4. Computed spatial distribution of the argon mass fraction in the plasma jet (outer line—0.1, contour interval—0.1; $y < 0$—lower semi-plane, $y > 0$—upper semi-plane).

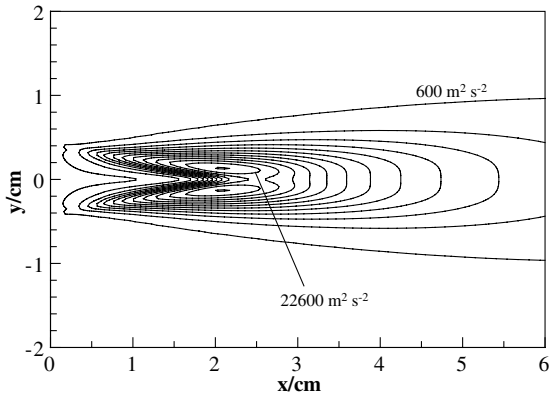

Fig. 5. Computed spatial distribution of the turbulent kinetic energy ($m^2 s^{-2}$) in the plasma jet (outer line—600 $m^2 s^{-2}$, contour interval—2000 $m^2 s^{-2}$; $y < 0$—lower semi-plane, $y > 0$—upper semi-plane).

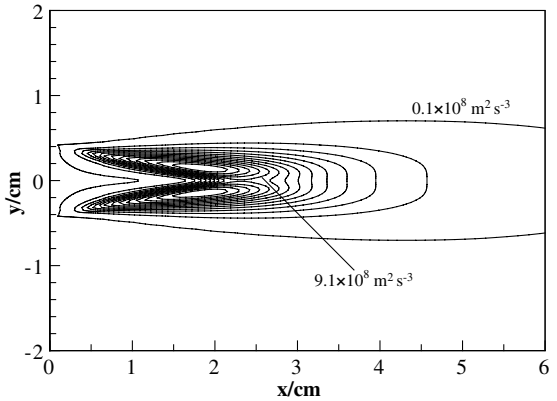

Fig. 6. Computed spatial distribution of the turbulence dissipation rate ($m^2 s^{-3}$) in the plasma jet (outer line—1×10^7 $m^2 s^{-3}$, contour interval—1×10^8 $m^2 s^{-3}$; $y < 0$—lower semi-plane, $y > 0$—upper semi-plane).

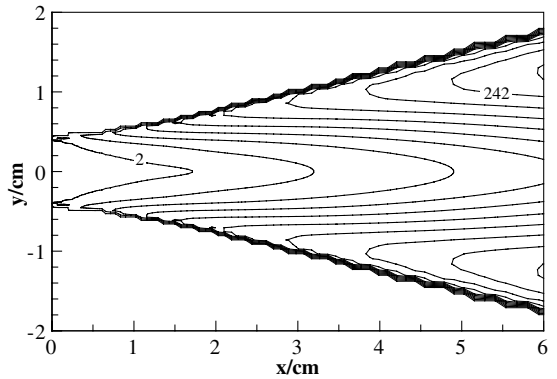

Fig. 7. Computed spatial distribution of the turbulent/molecular viscosity ratio (μ_t/μ) in the plasma jet (contour interval—30; $y < 0$—lower semi-plane, $y > 0$—upper semi-plane).

argon plasma jet indeed assumes much shorter high temperature region length, appreciably larger axial gradients of the plasma temperature and axial velocity (except for the region near the jet inlet), and much stronger entrainment of ambient air into the jet. For example, at the axial location about 4 cm downstream from the turbulent plasma jet inlet, the plasma axial velocity, temperature and argon mass fraction at the jet axis have reduced from ~1100 to ~300 m s^{-1}, from ~13 000 K to ~3000 K, and from 1.0 to ~0.4, respectively. On the other hand, corresponding modeling results for the long laminar argon plasma jet issuing into ambient air assume much smoother changes of those parameters along the jet axis [13].

Figs. 5–7 show that, as expected, the maximum values of the turbulent kinetic energy and its dissipation rate and comparatively large values of the turbulent/molecular viscosity ratio (μ_t/μ) all emerge in the mixing layer between the plasma jet and the ambient air where the radial gradient values of plasma velocity are comparatively large and thus turbulence generation terms are also large. However, the maximum values of the turbulent kinetic energy and its dissipation rate emerge at the locations not far from the jet inlet, whereas comparatively large values of the turbulent/molecular viscosity ratio (μ_t/μ) occur at the locations far from the jet inlet, where the gas temperatures have been comparatively low and thus the values of molecular viscosity are small.

Figs. 8–10 compare the present modeling results with corresponding experimental data [16,17] concerning the variations with the axial distance of the plasma axial velocity, temperature and air mole fraction at the jet axis. As is seen, the predicted axial variations of these plasma parameters are well consistent with corresponding experimental results. In those figures, the continuous line represents the predicted results of the axial velocity, temperature and air mole fraction along the jet axis when *both* turbulent and molecular diffusion mechanisms are included in the modeling, whereas the broken line is the calculated results when the combined ordinary and thermal diffusion coefficients are all taken to be zero

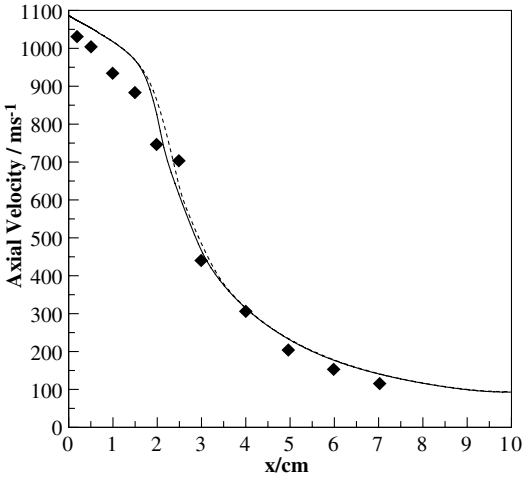

Fig. 8. Comparison of the computed results with corresponding experimental data [16,17] for the variation of axial velocity along the plasma axis. Continuous line—using the turbulence-enhanced combined-diffusion-coefficient method; broken line—only turbulent diffusion mechanism is considered.

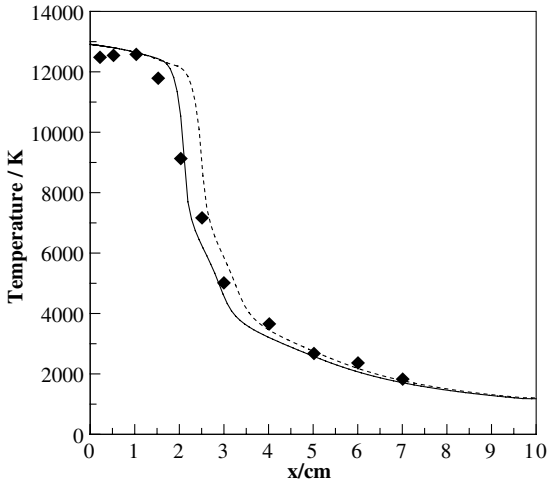

Fig. 9. Comparison of the computed results with corresponding experimental data [16,17] for the variation of plasma temperature along the plasma axis. Continuous line—using the turbulence-enhanced combined-diffusion-coefficient method; broken line—only turbulent diffusion mechanism is considered.

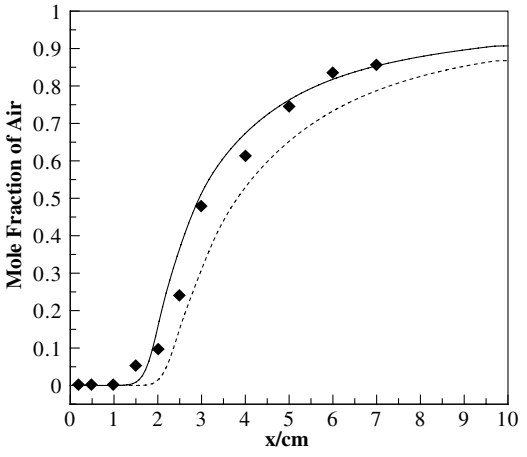

Fig. 10. Comparison of the computed results with corresponding experimental data [16,17] for the variation of air mole fraction along the plasma axis. Continuous line—using the turbulence-enhanced combined-diffusion-coefficient method; broken line—only turbulent diffusion mechanism is considered.

or *only* the turbulent diffusion mechanism is considered in the modeling. It can be seen that if the molecular diffusion mechanism is ignored, the predicted axial velocity variation in the jet is less affected, the calculated plasma temperatures at the jet axis are somewhat higher, while the values of the air mole fraction at the jet axis are appreciably underestimated. Hence, for the turbulent plasma jet under study, molecular diffusion mechanism (especially the effect of temperature gradient on species diffusion) cannot be ignored, and the present turbulence-enhanced combined-diffusion-coefficient approach can give good prediction concerning the entrainment of ambient air into the turbulent argon plasma jet.

Additional comparisons between the present modeling results and corresponding experimental data are presented in Figs. 11–13 concerning the radial profiles of the plasma axial velocity, temperature and air mole fraction at four different axial locations. It can also be seen that reasonable agreement is obtained between the present predicted results and the experimental data given in [16,17].

Ref. [17] studied the effects on the modeling results of a few different radial profiles of the turbulent kinetic energy at the jet inlet. It was shown that the initial turbulent kinetic energy level was critical, while the radial profile of the turbulent kinetic energy at the jet inlet was not important. In our modeling study, we also use the following expression as used in [17] to calculate the turbulent kinetic energy at the jet inlet

$$K = 0.000015U_0^2\left|\frac{\partial u}{\partial r}\Big/\left(\frac{\partial u}{\partial r}\right)_{\max}\right| \tag{19}$$

Eq. (19) is appreciably different from Eq. (15) used in the foregoing computation in their radial profiles. However,

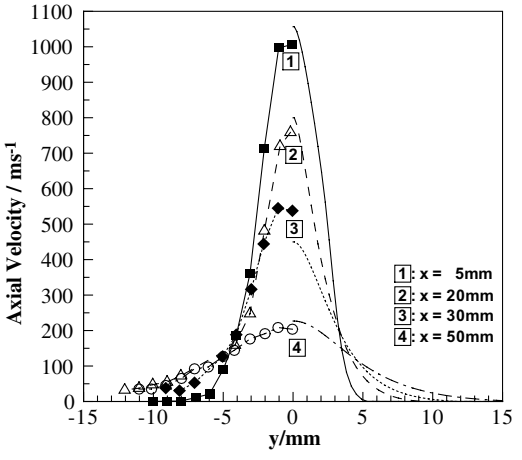

Fig. 11. Comparison of the computed results with corresponding experimental data for the radial distributions of the axial velocity at four different axial locations in the plasma jet. $y < 0$—experimental data [16,17], $y > 0$—modeling results.

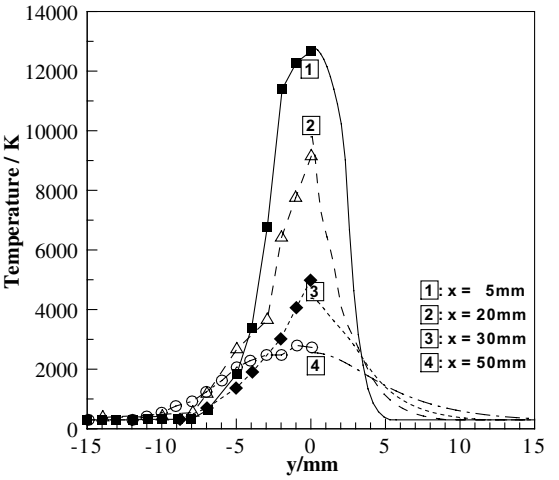

Fig. 12. Comparison of the computed results with corresponding experimental data for the radial distributions of the plasma temperature at four different axial locations in the plasma jet. $y < 0$—experimental data [16,17], $y > 0$—modeling results.

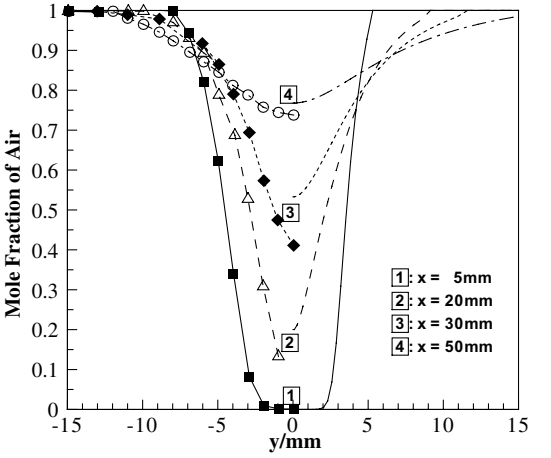

Fig. 13. Comparison of the computed results with corresponding experimental data for the radial distributions of the air mole fraction at four different axial locations in the plasma jet. $y < 0$—experimental data [16,17], $y > 0$—modeling results.

it is found that almost the same modeling results are obtained when either Eqs. (15) or (19) is used to calculate the turbulent kinetic energy at the jet inlet, implying that the profile form of the turbulent kinetic energy distribution at the jet inlet is indeed unimportant.

Density and temperature fluctuations have been ignored in the present modeling approach, although it is expected that besides the velocity fluctuations, density and temperature fluctuations also exist in the turbulent plasma jet. In order to take into account the density and temperature fluctuations in the turbulent plasma

flow, Chen et al. [20] and Merkhouf et al. [21] extended the standard K–ε two-equation turbulence model to a three-equation turbulence model using the density-weighted average quantities. However, comparison performed by Ye et al. [22] showed that almost the same modeling results were obtained by use of the two-equation and three-equation turbulence models, implying that the influence of density and temperature fluctuations was negligible under the plasma conditions. Hence, the standard K–ε two-equation turbulence model has been employed in the present study without accounting for the density and temperature fluctuations.

The flow picture of a practical turbulent plasma jet is extremely complex. Usually the random motion of arc-root at the anode surface of the plasma torch may cause the unsteadiness of the plasma jet [1,2]. The engulfment of cold ambient air at the fringes of the turbulent plasma jet can lead to the formation and dissipation of cold gas 'bubbles' in the jet [1,2,23]. It is anticipated that the K–ε two-equation turbulence model used in this study and in [17] may not well represent the actual processes. Hence, although the present study shows that the proposed modeling approach is useful in estimating the entrainment of ambient air into the turbulent plasma jet, it cannot be considered to be able to describe accurately the actual physical processes in turbulent plasma jets.

4. Conclusions

The turbulence-enhanced combined-diffusion-coefficient method is proposed and has been employed to study the entrainment of ambient air into the turbulent argon plasma jet. This modeling approach is much simpler than that used by the previous authors [17] because only the treatment of the diffusion between two different gases is required. Good agreement between the present predicted results and corresponding experimental data supports the employment of the turbulence-enhanced combined-diffusion-coefficient method.

Acknowledgments

This study was supported by the National Natural Science Foundation of China (Nos. 50176024, 50336010). The authors would like to thank Dr. A. B. Murphy, whose argon–air plasma properties have been used in this study.

References

[1] E. Pfender, Thermal plasma technology: where we stand and where are we going? Plasma Chem. Plasma Process. 19 (1) (1999) 1–31.

[2] P. Fauchais, A. Vardelle, Pending problems in thermal plasmas and actual development, Plasma Phys. Contr. Fus. 42 (Suppl. B) (2000) B365–B383.

[3] J. McKelliget, J. Szekely, M. Vardelle, P. Fauchais, Temperature and velocity fields in a gas flow exiting a plasma torch, Plasma Chem. Plasma Process. 2 (3) (1982) 317–332.

[4] Y.C. Lee, E. Pfender, Particle dynamics and particle heat and mass transfer in thermal plasmas. Part III. Thermal plasma jet reactors and multiparticle injection, Plasma Chem. Plasma Process. 7 (1) (1987) 1–27.

[5] Y.P. Chyou, E. Pfender, Modeling of plasma jets with superimposed vortex flow, Plasma Chem. Plasma Process. 9 (2) (1989) 291–328.

[6] C.H. Chang, J.D. Ramshaw, Numerical simulations of argon plasma jets flowing into cold air, Plasma Chem. Plasma Process. 13 (2) (1993) 189–209.

[7] A. Vardelle, P. Fauchais, B. Dussoubs, N.J. Themelis, Heat generation and particle injection in a thermal plasma torch, Plasma Chem. Plasma Process. 18 (4) (1998) 551–574.

[8] H.-P. Li, Xi Chen, Three-dimensional modeling of the turbulent plasma jet impinging upon a flat plate and with transverse particle and carrier-gas injection, Plasma Chem. Plasma Process. 22 (1) (2002) 27–58.

[9] K. Ramachandran, H. Nishiyama, Three-dimensional effects of carrier gas and particle injection on the thermo-fluid fields of plasma jets, J. Phys. D: Appl. Phys. 35 (4) (2002) 307–317.

[10] K. Osaki, O. Fugumasa, A. Kobayashi, High thermal efficiency-type laminar plasma jet generator for plasma processing, Vacuum 59 (1) (2000) 47–54.

[11] W.X. Pan, W. Hua Zhang, W. Hong Zhang, C.K. Wu, Generation of long, laminar plasma jets at atmospheric pressure and effects of flow turbulence, Plasma Chem. Plasma Process. 21 (1) (2001) 23–35.

[12] W.X. Pan, W.H. Zhang, W. Ma, C.K. Wu, Characteristics of argon laminar DC plasma jet at atmospheric pressure, Plasma Chem. Plasma Process. 22 (2) (2002) 271–283.

[13] D.-Y. Xu, Xi Chen, K. Cheng, Three-dimensional modeling of the characteristics of long laminar plasma jets with lateral injection of carrier gas and particulate matter, J. Phys. D: Appl. Phys. 36 (13) (2003) 1583–1594.

[14] A.B. Murphy, Diffusion in equilibrium mixtures of ionized gases, Phys. Rev. E 48 (5) (1993) 3594–3603.

[15] A.B. Murphy, A comparison of treatments of diffusion in thermal plasmas, J. Phys. D: Appl. Phys. 29 (7) (1996) 1922–1932.

[16] J.R. Fincke, D.M. Crawford, S.C. Snyder, W.D. Swank, D.C. Haggard, R.L. Williamson, Entrainment in high-velocity, high-temperature plasma jets, Part I: Experimental results, Int. J. Heat Mass Transfer 46 (22) (2003) 4201–4213.

[17] R.L. Williamson, J.R. Fincke, D.M. Crawford, S.C. Snyder, W.D. Swank, D.C. Haggard, Entrainment in high-velocity, high-temperature plasma jets, Part II: computational results and comparison to experiment, Int. J. Heat Mass Transfer 46 (22) (2003) 4215–4228.

[18] P. Han, Numerical and experimental studies on the characteristics of D.C. arc plasma torches and jets, Ph.D. Thesis, Tsinghua University, Beijing, China, 1999 (in Chinese).

[19] S.V. Patankar, Numerical Heat Transfer and Fluid Flow, Hemisphere, Washington, 1980, pp. 115–146.
[20] Xi Chen, A. Merkhouf, M.I. Boulos, Preliminary study of the 3-equation turbulence model of an R.F. plasma torch, in: Proceedings of the Third Asia-Pacific Conference on Plasma Science and Technology, vol. 1, Tokyo, Japan, 1996, pp. 71–76.
[21] A. Merkhouf, R. Ye, P. Proulx, M.I. Boulos, Mathematical model of plasma system, in: Proceedings of the Julian Szekely Memorial Symposium on Materials Processing, Boston, USA, 1997, pp. 509–528.
[22] R. Ye, P. Proulx, M.I. Boulos, Turbulence phenomena in the radio frequency induction plasma torch, Int. J. Heat Mass Transfer 42 (9) (1999) 1585–1595.
[23] R. Spores, E. Pfender, Flow structure of a turbulent thermal plasma jet, Surf. Coat. Technol. 37 (3) (1989) 251–270.